Fullerene-based ruthenium catalysts: a novel approach for anchoring metal to carbonaceous supports. I. Structure

Th. Braun, M. Wohlers, T. Belz, G. Nowitzke [a], G. Wortmann [a], Y. Uchida, N. Pfänder and R. Schlögl

Fritz-Haber-Institut der Max-Planck-Gesellschaft, Faradayweg 4-6, 14195 Berlin, Germany
[a] *Fachbereich Physik, Universität-GH Paderborn, 33095 Paderborn, Germany*

Received 13 August 1996; accepted 22 October 1996

The influence of fullerenes and related support materials on the structural and catalytic properties of ruthenium was investigated. Catalysts based on C_{60}, raw fullerene black, extracted fullerene black, cathode deposit and graphite were prepared by an impregnation/activation procedure with Ru_3CO_{12}. The local co-ordination sphere of the resulting highly dispersed X-ray amorphous ruthenium was investigated by means of EXAFS. The dominating role of the presence of non-six-membered carbon rings on the structure and the stability of the Ru particles will be illustrated.

Keywords: fullerenes, fullerene black, cathode deposit, ruthenium, EXAFS

1. Introduction

Supported transition metals are commonly applied in heterogeneous catalysis. Various carbonaceous substances like active carbon, charcoal, carbon black, and graphite are support materials of significant interest. These materials differ in their chemical and physical properties, like total surface area, chemical stability of the bulk material and functional groups at the surface, which affect the metal–support interaction [1]. A new class of carbonaceous substances, the fullerenes, recently gained interest concerning their potential application as support materials in heterogeneous catalysis [2–7]. The fullerenes exhibit exceptional structural and chemical properties that differ markedly from conventional carbonaceous materials.

Fullerenes are produced by the electric arc graphite evaporation process according to Krätschmer and Huffman [8]. The synthesis conditions lead to the formation of two different raw products namely fullerene black and cathode deposit. Fullerene black is found on the chamber surfaces whereas cathode deposit arises on the hot negative-charged graphite rod. Their different formation conditions induce distinctive structural properties [9]. Cathode deposit is built of tangled or twisted graphene layers, multi-shelled nanoparticles, multi-shelled nanotubes, and graphitic units. The X-ray amorphous fullerene black mainly consists of smoothly bent carbon material containing a high amount of spherical fragments. Up to 11 wt% extractable molecular fullerenes are highly dispersed on this carbon material [10]. Considering the well known structural features of carbon nanotubes [11] and molecular fullerenes [12], the presence of five- or seven-membered carbon rings in the insoluble fraction of fullerene black and cathode deposit has to be assumed.

Five-membered rings being present in all molecular fullerenes like C_{60} or C_{70} alter the reactivity of adjacent double bonds. In C_{60} they can form η^2-type chemical bonds to zero-valent transition metals [13,14]. The chemistry of fullerenes and fullerene black should therefore cause an interaction between the metal and the substrate which is different from the interaction of conventional carbon materials with metal particles.

The aim of this work was to elucidate the specific influence of carbonaceous support materials on the structural properties of different ruthenium/carbon systems. The substances, which are based on raw fullerene black (Ru-FBnex, i.e. ruthenium on not extracted fullerene black), toluene extracted fullerene black (Ru-FBex, i.e. ruthenium on extracted fullerene black), cathode deposit (Ru-CD, i.e. ruthenium on cathode deposit), and graphite (Ru-AFS, i.e. ruthenium on AFS-graphite), were prepared by a combined impregnation/activation reaction which is based on the thermally induced decomposition of $Ru_3(CO)_{12}$ in boiling toluene. An analogously prepared C_{60}-ruthenium compound, denoted as Ru_3C_{60}, because of its formal stoichiometry, served as a model substance for molecular fullerene-containing systems.

2. Experimental

All fullerene materials were produced in a BUCKY-II apparatus (Ulvick Industries) using high-purity graphite rods (Ringsdorff RW4, 99.99% C). Commercially available graphite (AFS, Kropfmühl AG) was used. All catalysts were prepared under strict

exclusion of air using the Schlenck-technique. Ru_3C_{60} was prepared by slow addition of one equivalent of $Ru_3(CO)_{12}$ (959 mg) to a solution of C_{60} (1080 mg, 1.5 mmol) in 500 ml toluene. The resulting brown suspension was slowly heated to reflux under vigorous stirring for a period of three days. After cooling to room temperature the insoluble black product was filtered off and was washed subsequently with toluene and ether. Neither C_{60} nor ruthenium was found in the filtrates. The solid reaction product was dried in vacuo at room temperature. The carbon-supported ruthenium catalysts were prepared by addition of $Ru_3(CO)_{12}$ (959 mg) to toluene (500 ml) suspensions of the respective carbon materials (3 g) under argon. The resulting reaction mixtures were heated to reflux for 24 h. After cooling to room temperature the catalysts were isolated by filtration, subsequent washing with toluene and ether and a drying procedure in vacuo at room temperature.

Energy dispersive X-ray fluorescence analysis (Seiko Industries SEA 2010) was used to determine the ruthenium content of all samples.

EXAFS (extended X-ray adsorption fine structure) data were collected at the RÖMO-II beamline of HASYLAB using a Si-(311) double crystal monochromator. Energy calibration was performed by measuring a ruthenium powder sample as reference absorber. All EXAFS-spectra were recorded at room temperature.

TEM (transmission electron microscopy) images were taken on a Philips EM 400 T, a Siemens EM 102 and a Phillips CM 200 FEG transmission microscope. BET surface areas were determined after annealing the samples in vacuo at 523 K for 16 h (Quantasorb Junior, Quantachrom). Hydrogen uptakes were measured after annealing the samples in vacuo at 673 K for 16 h (Autosorb 1, Quantachrom).

3. Results

The structures of all catalysts were investigated by means of TEM to determine their morphology and EXAFS to gain information about the local co-ordination sphere of ruthenium. The behaviour of the catalysts against thermal treatment in inert and reductive atmosphere was observed. Distinctive effects of the different support materials on the structure and the stability of the present ruthenium species were found.

3.1. Characterisation of the pristine catalysts

The ruthenium contents of all catalysts were determined by X-ray fluorescence. Table 1 summarises the ruthenium weight percentages and the abbreviations used for the different ruthenium/carbon systems.

As a result of the preparation procedure all compounds were found to contain residual solvent which was not removed by the drying process. Furthermore, IR-spectroscopy proved the presence of CO co-ordinated to ruthenium which can be traced back to the used metal precursor $Ru_3(CO)_{12}$.

Powder X-ray diffraction indicated that all compounds were amorphous with respect to the present ruthenium species, thus excluding the formation of large crystalline metal particles during the preparation. TEM images revealed the presence of small (2–5 nm) ruthenium particles in all catalysts (see table 1).

More structural information about the X-ray amorphous and morphologically not distinguishable ruthenium particles in the different samples was gained by means of EXAFS-measurements at the K-edge of ruthenium. The k^2-weighted Fourier transforms of the respective X-ray absorption spectra provide the possibility of a qualitative comparison of structural properties of the different ruthenium species (fig. 1). Considering the EXAFS data of $Ru_3(CO)_{12}$, RuO_2, and ruthenium metal, the sole presence of crystalline ruthenium metal, RuO_2 or of unreacted $Ru_3(CO)_{12}$ in any of the catalysts has to be ruled out.

The almost identical EXAFS data of $Ru_3(CO)_{12}$ and a compound which was prepared from a solution of C_{60} and $Ru_3(CO)_{12}$ in toluene at room temperature (denoted as C_{60}-$Ru_3(CO)_{12}$-RT) clearly point out that thermal

Table 1
Characterisation of the catalysts

Sample abbreviation	Support	Ru [a] (wt%)	BET support [b] (m^2/g)	BET catalyst [b] (m^2/g)	Particle ⌀ pristine [c] (nm)	Particle ⌀ annealed 573 K [c] (nm)	Particle ⌀ after CO hyd. 573 K [c] (nm)
Ru_3C_{60}	C_{60}	20	~ 5	191	2	3	~ 5
Ru-FBnex	not extracted fullerene black	3.5	295	232	3	4	~ 10
Ru-FBex	extracted fullerene black	4	325	269	2	3	4
Ru-CD	cathode deposit	2	35	22	2	3	3
Ru-AFS	AFS-graphite	2.8	1.2	12	2	–	–

[a] Determined by X-ray fluorescence analysis.
[b] Measured after annealing in vacuo at 523 K.
[c] Determined by TEM.

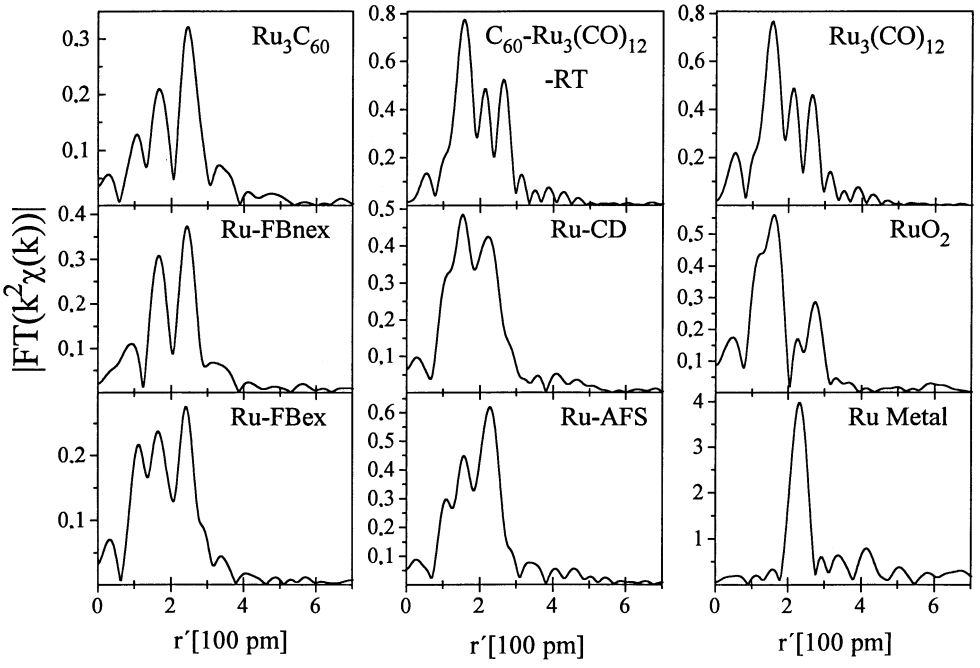

Fig. 1. Fourier transforms of the ruthenium K-edge absorption spectra after k^2-weighting. Pristine catalysts.

treatment during the synthesis inducing the decomposition of $Ru_3(CO)_{12}$ is essential for the evolution of the observed ruthenium species in Ru_3C_{60}. These species were shown to be CO-containing ruthenium clusters which are chemically bonded to C_{60} units [2]. The formation of a network built of C_{60} units that are interlinked by ruthenium clusters caused the high total surface area (table 1) of Ru_3C_{60}.

The quite similar Fourier transforms of Ru_3C_{60} and Ru-FBnex (fig. 1) were explained by a structure model for Ru-FBnex that proposed the presence of Ru_x(fullerene)$_y$ compounds adsorbed on fullerene black. This Ru_x(fullerene)$_y$ originated from the dissolution of mainly C_{60} and higher fullerenes out of the not extracted fullerene black during the preparation and the subsequent reaction of these molecular fullerenes with ruthenium species. This model is confirmed by comparison of the Fourier transforms of Ru-FBnex with those of Ru_3C_{60} and Ru-FBex (fig. 1). The latter revealed the presence of ruthenium in Ru-FBex which is co-ordinated different from the former two catalysts. In Ru-FBnex the presence of significant amounts of ruthenium species which are similar to those observed in Ru-FBex was excluded. The interaction between the insoluble fraction of the fullerene black and the ruthenium species in Ru-FBnex was therefore excluded to be the determining factor for the structure of the present ruthenium species.

A comparison of the Fourier transforms of Ru-CD and Ru-AFS with those of metallic ruthenium and ruthenium oxide led to the assumption that both catalysts contain metal-like and oxide-like ruthenium species in different amounts.

In contrast to Ru_3C_{60}, Ru-FBnex, and Ru-FBex these ruthenium particles do not obey a homogeneous spatial distribution. TEM images of Ru-AFS (fig. 2) revealed a preferential location of the ruthenium particles along prismatic faces of the graphite flakes. The strongly inhomogeneous nature of the cathode deposit was reflected by the existence of domains containing no ruthenium and areas where the accumulation of ruthenium particles was observed (fig. 2).

HRTEM of Ru-CD

The most abundant structural features in the cathode deposit used in this study were graphene units of different sizes which are often curved or bent. Spherical or polygonal multi-shelled graphitic nanoparticles were frequently observed whereas carbon nanotubes were hardly found. Most likely due to the different compositions of the used carbon deposits, the previously reported formation of metallic ruthenium on the outer surfaces of carbon nanotubes [3] was rarely observed. Only a negligible amount of ruthenium particles was detected directly attached to carbon nanotubes or to carbon nanoparticles. Basal faces, prismatic faces, and visible defects of the graphene units exhibited a markedly low affinity for ruthenium.

HRTEM images of Ru-CD (fig. 2) revealed the coincidence of distinctive structural features in typical bonding sites for ruthenium. The intersection of several graphene units forms a cavity. The ruthenium particles were found to be preferentially attached at curved graphene layers inside the cavities. The curvatures of the graphene layers are most likely caused by five- or seven-membered carbon rings which enhance the reactivity of the adjacent double bonds thus affecting the interaction

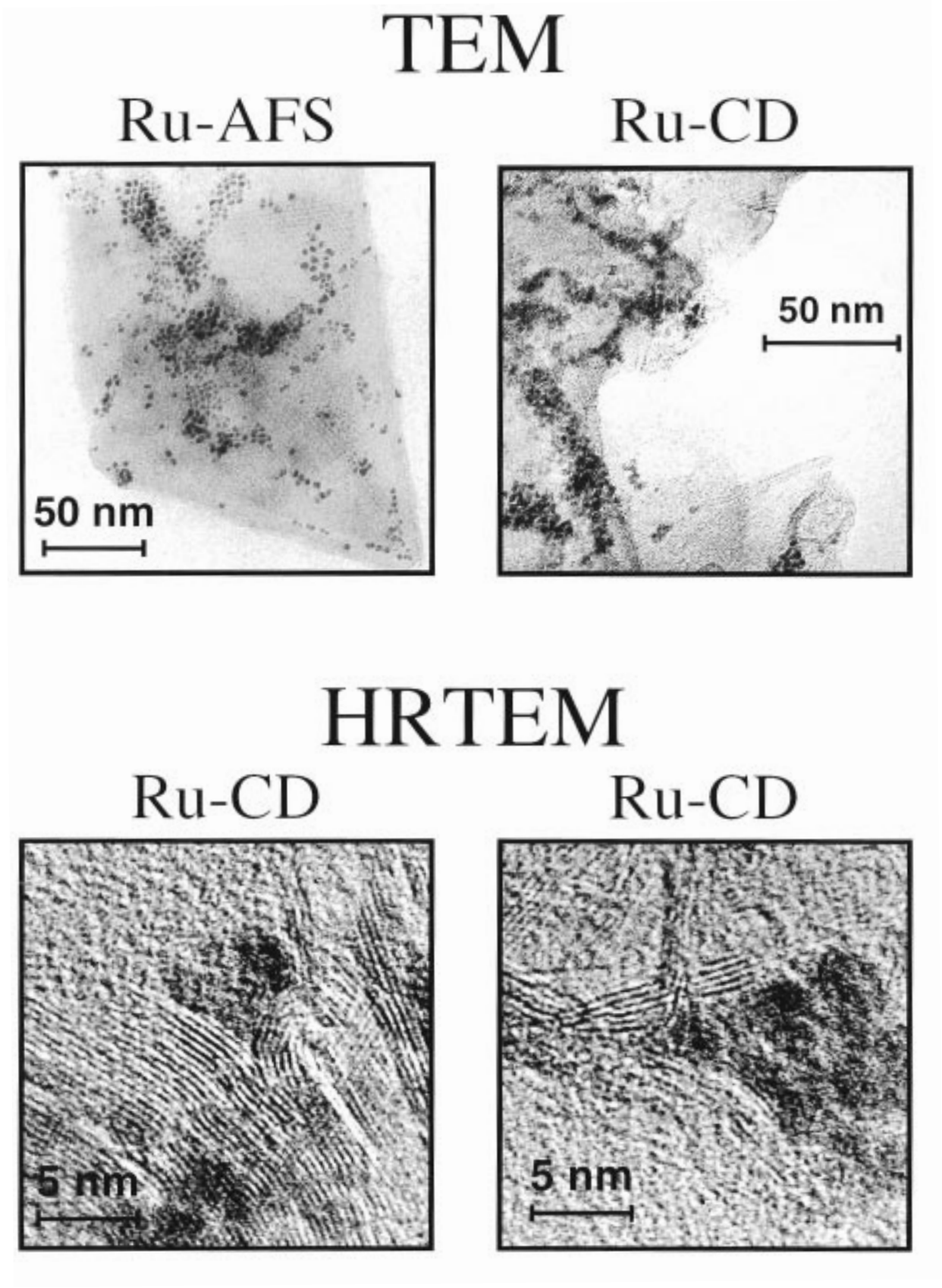

Fig. 2. TEM images of Ru-AFS and Ru-CD; HRTEM images of Ru-CD.

between the cathode deposit and the ruthenium particles.

3.2. Characterisation of catalysts annealed in vacuo

The thermal behaviour of the ruthenium species present in the catalysts was examined by EXAFS and TEM of samples that had been annealed at 573 K in vacuo (10^{-6} mbar).

Temperature-programmed desorption (TPD) experiments confirmed the desorption of CO upon thermal treatment in inert atmosphere. Previous studies [2] on the thermal behaviour of Ru_3C_{60} revealed that the desorption of residual CO ligands at 870 K caused the formation of a metal surface which is capable of CO adsorption. The ruthenium particles retain their morphology whereas the dissociation of CO led to a partial oxidation of the C_{60} molecules.

The average diameter (table 1) and the morphology of the ruthenium species on the respective supports were determined before and after annealing by TEM. A slightly increased diameter of the spherical ruthenium particles was observed on all supports with the exception of Ru-AFS. Where commencing agglomeration processes led to a bimodal particle size distribution consisting of slightly enlarged spherical ruthenium particles (2–3 nm) and irregularly shaped ruthenium islands (10–20 nm).

The EXAFS data of the previously annealed catalysts are shown in fig. 3. The Fourier transforms of Ru-AFS and Ru-CD clearly indicate the evolution of ruthenium metal co-ordinated to carbon upon thermal treatment, whereas the spectra of the ruthenium species in all other catalysts remain nearly unchanged. The formation of significant amounts of well defined metal crystallites on Ru_3C_{60}, Ru-FBnex, and Ru-FBex after annealing at 573 K can be ruled out. However, the observed minor changes of their Fourier transforms indicate re-crystallisation and de-bonding from the substrate. This hypothesis was confirmed by the EXAFS data of Ru_3C_{60} annealed in vacuo at 873 K (fig. 3) which clearly revealed the formation of ruthenium metal.

Furthermore, the formation of metal surfaces after annealing at 673 K was proved by the adsorption of hydrogen at room temperature. However, only Ru_3C_{60} and Ru-FBnex exhibited a Langmuir-type adsorption isotherm. Their chemisorption data revealed the metal surface area of the catalysts being approximately two orders of magnitude smaller than the values estimated according to the particle diameter after annealing at 573 K. The complex hydrogen adsorption behaviour of Ru-FBex, Ru-CD, and Ru-AFS might be explained by hydrogen spill-over phenomena and/or reaction of hydrogen with absorbed species on the ruthenium surface. However, on all catalysts only a small fraction of the ruthenium surface is accessible for hydrogen adsorption.

3.3. Characterisation of the catalysts after CO hydrogenation

During the CO hydrogenation the catalysts are exposed to a reductive atmosphere de-stabilising the particle dispersion. All catalysts were investigated after

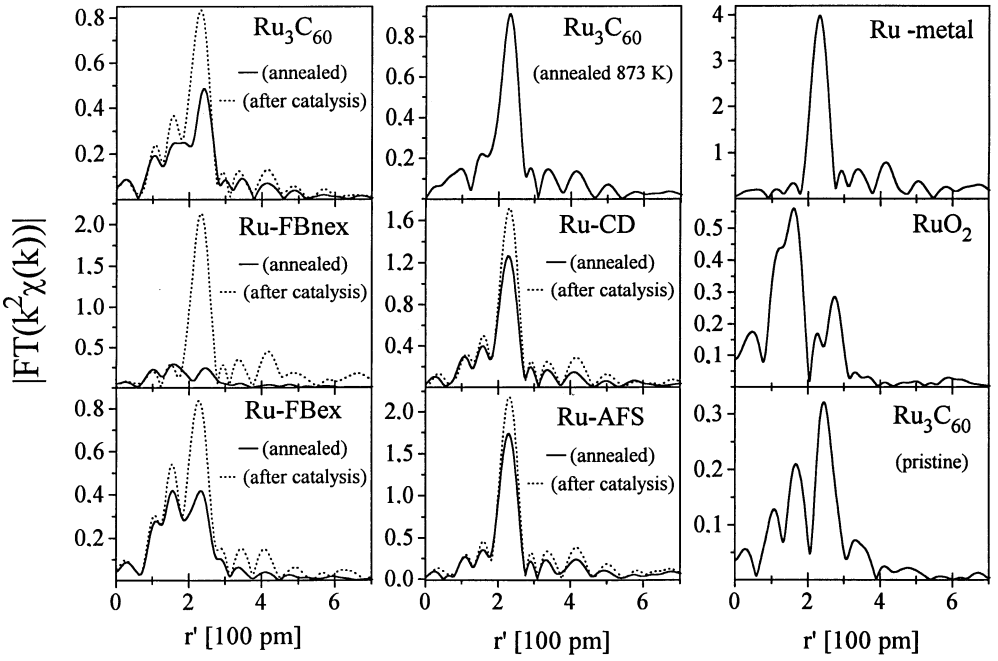

Fig. 3. Fourier transforms of the ruthenium K-edge absorption spectra after k^2-weighting. (—) Catalysts after annealing at 573 K in vacuo; (···) catalysts after CO hydrogenation at 573 K.

prolonged use (over 200 h on stream) in the CO hydrogenation at 573 K.

TEM images revealed enlarged ruthenium particles (table 1) in all used catalysts. The morphologies of the ruthenium particles in Ru_3C_{60} and Ru-FBnex were affected by the chemical potential of the atmosphere during thermal treatment. In contrast to the samples which were annealed in vacuo, Ru_3C_{60} and Ru-FBnex contained well crystallised ruthenium metal particles after use in the CO hydrogenation. TEM images of Ru-FBnex showed rarely spherical but predominantly hexagonal ruthenium metal particles. Unlike Ru-FBnex, Ru_3C_{60} contains a mixture of amorphous ruthenium particles and ruthenium metal crystallites which are preferentially located at the outer surfaces of the compound. TEM images of Ru-FBex exhibited an enlarged average diameter of the spherical ruthenium particles after CO hydrogenation compared to the samples annealed in vacuo.

TEM images of Ru-AFS and Ru-CD revealed morphological nearly identical ruthenium species irrespective of the atmosphere during the temperature treatment. This finding accords with the EXAFS data (fig. 3) proofing the formation of metallic ruthenium on Ru-CD and Ru-AFS as well after annealing in vacuo as after use in the CO hydrogenation.

The EXAFS Fourier transforms of Ru_3C_{60}, Ru-FBnex, and Ru-FBex after CO hydrogenation are shown in fig. 3. The comparison of the Fourier transforms of ruthenium metal and Ru-FBnex confirm the presence of well crystallised ruthenium metal in Ru-FBnex. Furthermore, the EXAFS data revealed the formation of metallic ruthenium species on Ru-FBex and Ru_3C_{60} during the CO hydrogenation.

In the used catalysts not all of the ruthenium is present as bulk metal indicating either some residual covalent interaction to the substrate or compound formation after termination of the catalytic testing. Such degradation would point to an extreme chemical reactivity of the Ru particles.

The data in fig. 3 further show that reductive catalysis is much stronger a restructuring process than thermal annealing alone.

4. Discussion

The characterisation of the catalysts clearly revealed that the structure and the reactivity of the ruthenium species depend on the respective carbonaceous support material. All catalysts contain a distribution of highly dispersed ruthenium species with distinctive structural features induced by the respective support material. The sole presence of ruthenium oxide, metallic ruthenium, or $Ru_3(CO)_{12}$ was ruled out by the EXAFS data.

According to the local co-ordination of ruthenium and their catalytic behaviour, which will be discussed in detail in the second part of this contribution, the catalysts can be separated into two groups: Ru-CD and Ru-AFS which contain mainly oxide-like and metal-like ruthenium species and Ru_3C_{60}, Ru-FBnex, and Ru-FBex.

The exact structure of the ruthenium species in Ru_3C_{60}, Ru-FBnex, and Ru-FBex is not known, but the predominant presence of ruthenium clusters which contain residual CO ligands ($Ru_x(CO)_y$) was indicated by IR-spectroscopy and TPD experiments. In Ru_3C_{60} these ruthenium clusters are bonded to fullerene molecules [2] building a network of linked C_{60} units with a high total surface area. Based on the nearly identical EXAFS spectra of Ru_3C_{60} and Ru-FBnex it was concluded that the $Ru_x(CO)_y$ clusters are also chemically bonded to molecular fullerene units in Ru-FBnex. This high reactivity of molecular fullerenes with respect to ruthenium was attributed to the presence of five-membered carbon rings which determine the chemical behaviour of their adjacent double bonds. In C_{60} these electron deficient double bonds are known to form η^2-type transition-metal complexes [13]. Extracted fullerene black and cathode deposit contain analogous features, e.g. carbon rings that are not built of six carbon atoms (henceforth referred to as non-six-membered carbon rings: NSMCR). They cause the formation of curved units containing reactive carbon–carbon double bonds which are assumed to possess a similar reactivity to ruthenium like the carbon–carbon double bonds in molecular fullerenes.

The preferred bonding of ruthenium to fullerene-like structures in Ru-FBex was deduced from the catalytic properties and the behaviour during thermal treatment which correspond to Ru_3C_{60} and Ru-FBnex. In contrast to Ru-AFS and Ru-CD the chemical potential of the atmosphere during thermal treatment influenced the structural changes of the ruthenium species in Ru_3C_{60}, Ru-FBnex, and Ru-FBex. Annealing in vacuo at 573 K caused the formation of metallic ruthenium in Ru-AFS and Ru-CD whereas only minor structural changes of the ruthenium species in Ru_3C_{60}, Ru-FBnex, and Ru-FBex were observed. The formation of metallic ruthenium in Ru_3C_{60}, Ru-FBnex, and Ru-FBex occurred after prolonged use in the CO hydrogenation. The degree of crystallisation during the catalysis varied with the support. Well defined ruthenium metal crystallites exhibiting hexagonal morphology were the most abundant species in Ru-FBnex, present in Ru_3C_{60}, and not found in Ru-FBex. It is assumed that the loss of redundant CO ligands induces crystallisation processes of the $Ru_x(CO)_y$ species and the cleavage of metal–support interactions enables the agglomeration of reactive ruthenium clusters. Considering the nearly unchanged morphology of the ruthenium particles in Ru_3C_{60}, Ru-FBnex, and Ru-FBex after annealing in inert atmosphere the reductive degradation of the support material seems to be

responsible for the increased formation of ruthenium metal crystallites during catalysis.

Significant reactions of the support materials in Ru-CD and Ru-AFS which influence the agglomeration processes were excluded, because different chemical potentials of the atmosphere hardly altered the morphologies and the co-ordination sphere of the ruthenium species formed upon thermal treatment. Although the slightly different total surface areas of the two catalysts might affect the agglomeration behaviour, the high dispersion of the ruthenium particles on cathode deposit after thermal treatment was mainly attributed to the higher stability of the ruthenium–support interaction in Ru-CD compared to Ru-AFS. A unique feature of carbon deposit as support is the coexistence of NSMCR in pocket sites of the secondary structure of the nanocarbon allowing for the co-ordinated action of chemical bonding of Ru clusters and their mechanical fixation.

The structural characterisation of the catalysts allowed the conclusion that the NSMCR which are unique to fullerene carbon are important to stabilise small Ru clusters. They remain covalently bonded to the carbon at medium-high temperatures. This state which is a catalyst in its own right is also a precursor to another catalyst with small Ru particles supported on the carbonaceous substrate. Both types of catalysts differ in their CO hydrogenation performances as will be discussed in part II of this contribution [15].

Carbons with a high NSMCR abundance (more than one NSMCR per particle) stabilise Ru clusters effectively but are susceptible to reductive degradation by hydrogen spill-over. They are less stable at higher reaction temperatures. Carbons with a low NSMCR abundance can stabilise the Ru clusters less effectively but are more stable towards reductive degradation. A significant dispersion of the ruthenium particles can be maintained on a mesostructure of multiply curved nanocarbons which provide a pocket surface without micro-porosity. The cathode deposit nanocarbon is a good combination of the strongly corrugated surface with pockets for particles and high local diffusion barriers and a low abundance of NSMCR rendering the surface secondary structure robust against flattening by reductive degradation. This direction of optimisation offers a wide range of preparative variants of potentially useful and cheaply available novel nanocarbons.

Acknowledgement

This work was supported by the Bundesministerium für Bildung und Forschung through its fullerene programme.

References

[1] D. Cameron, S. Cooper, I. Dodgson, B. Harrison and J. Jenkins, Catal. Today 7 (1990) 113.
[2] M. Wohlers, B. Herzog, T. Belz, A. Bauer, Th. Braun, Th. Rühle and R. Schlögl, Synth. Met. 77 (1996) 55.
[3] J.M. Planeix et al., J. Am. Chem. Soc. 116 (1994) 7935.
[4] H. Nagashima, A. Nakaoka, Y. Saito, M. Kato, T. Kawanishi and K. Itoh, Chem. Soc. Chem. Commun. (1992) 377.
[5] H. Nagashima, H. Yamaguchi, Y. Kato, Y. Saito and K. Itoh, Chem. Lett. (1993) 2153.
[6] H. Nagashima, A. Nakaoka, S. Tajima, Y. Saito and K. Itoh, Chem. Lett. (1992) 1361.
[7] H. Nagashima, Y. Kato, H. Yamaguchi, E. Kimura, T. Kawanishi, M. Kato, Y. Saito, M. Haga and K. Itoh, Chem. Lett. (1994) 1207.
[8] W. Krätschmer, L. Lamb, K. Frostiropoulos and D.R. Huffman, Nature 347 (1990) 345.
[9] T. Belz, J. Find, D. Herein, N. Pfänder, T. Rühle, H. Werner, M. Wohlers and R. Schlögl, Ber. Bunsenges. Phys. Chem., submitted (1996).
[10] M. Kanowski, H.-M. Vieth and K. Lüders, Carbon, submitted (1996).
[11] M.S. Dresselhaus, Nature 358 (1992) 195.
[12] W. Bensch, H. Werner, H. Bartl and R. Schlögl, J. Chem. Soc. Faraday Trans. 90 (1994) 2791.
[13] M. Rasinkangas, T.T. Pakkanen and T.A. Pakkanen, J. Organomet. Chem. 476 (1994) C6.
[14] P.J. Fagan, J.C. Calabrese and B. Malone, Acc. Chem. Res. 25 (1992) 134.
[15] Th. Braun, M. Wohlers, T. Belz and R. Schlögl, Catal. Lett. 43 (1997) 175.